Report

Cell Reports

Synapse Formation Activates a Transcriptional Program for Persistent Enhancement in the Bi-directional Transport of Mitochondria

Graphical Abstract

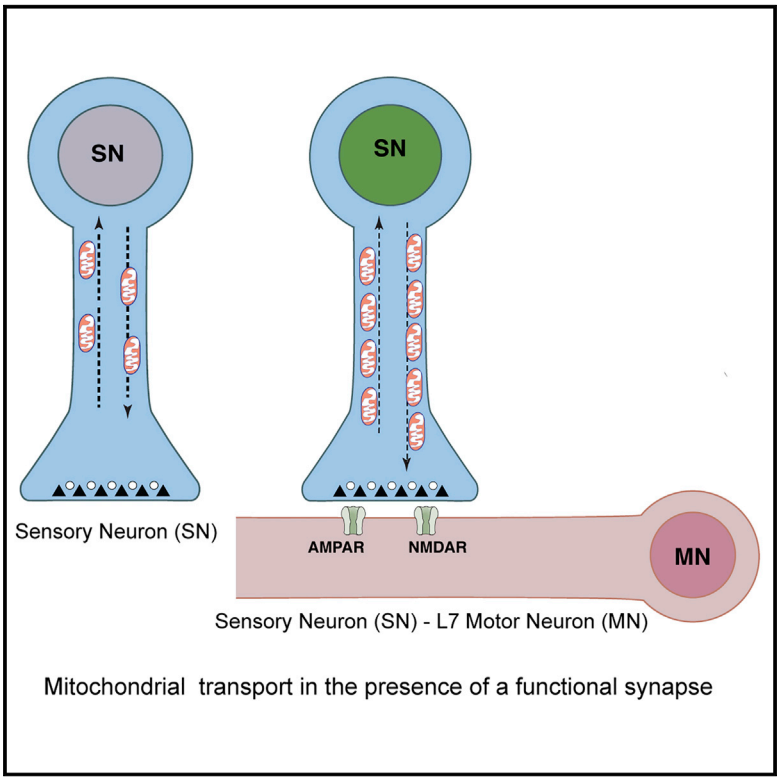

Authors

Kerriann K. Badal, Komol Akhmedov, Phillip Lamoureux, ..., Supriya Swarnkar, Kyle E. Miller, Sathyanarayanan V. Puthanveettil

Correspondence

sputhanv@scripps.edu

In Brief

Badal et al. show that the formation of a functional synapse between pre-synaptic sensory and post-synaptic motor neurons of the gill withdrawal reflex of *Aplysia* results in persistently enhanced anterograde and retrograde transport of mitochondria in sensory neurons. Once synapses are formed, transcription and translation in pre-synaptic neurons constrain mitochondrial transport.

Highlights

- Synapse formation produces persistent enhancements in mitochondrial transport
- The enhancements in mitochondrial transport depend on cAMP-PKA signaling
- Persistently enhanced mitochondrial transport requires transcription and translation
- Synapse formation results in persistent changes in the pre-synaptic transcriptome

Badal et al., 2019, Cell Reports *26*, 507–517
January 15, 2019
https://doi.org/10.1016/j.celrep.2018.12.073

CellPress

Cell Reports
Report

Synapse Formation Activates a Transcriptional Program for Persistent Enhancement in the Bi-directional Transport of Mitochondria

Kerriann K. Badal,[1,4] Komol Akhmedov,[1] Phillip Lamoureux,[2] Xin-An Liu,[1,5] Adrian Reich,[3] Mohammad Fallahi-Sichani,[3] Supriya Swarnkar,[1] Kyle E. Miller,[2] and Sathyanarayanan V. Puthanveettil[1,6,*]
[1]Department of Neuroscience, The Scripps Research Institute-Florida, 130 Scripps Way, Jupiter, FL 33458, USA
[2]Department of Integrative Biology, Michigan State University, East Lansing, MI 48824, USA
[3]Bioinformatics Core, The Scripps Research Institute-Florida, 130 Scripps Way, Jupiter, FL 33458, USA
[4]Integrative Biology PhD Program, Charles E. Schmidt College of Science, Florida Atlantic University, Jupiter, FL 33458, USA
[5]Present address: Department of Neuroscience, Icahn School of Medicine at Mount Sinai, New York, NY, USA
*Correspondence: sputhanv@scripps.edu
https://doi.org/10.1016/j.celrep.2018.12.073

SUMMARY

Mechanisms that regulate the bi-directional transport of mitochondria in neurons for maintaining functional synaptic connections are poorly understood. Here, we show that in the pre-synaptic sensory neurons of the *Aplysia* gill withdrawal reflex, the formation of functional synapses leads to persistent enhancement in the flux of bi-directional mitochondrial transport. In the absence of a functional synapse, activation of cAMP signaling is sufficient to enhance bi-directional transport in sensory neurons. Furthermore, persistent enhancement in transport does not depend on NMDA and AMPA receptor signaling nor signaling from the post-synaptic neuronal cell body, but it is dependent on transcription and protein synthesis in the pre-synaptic neuron. We identified ~4,000 differentially enriched transcripts in pre-synaptic neurons, suggesting a long-term change in the transcriptional program produced by synapse formation. These results provide insights into the regulation of bi-directional mitochondrial transport for synapse maintenance.

INTRODUCTION

Synapse formation requires the coordinated regulation of molecular and biochemical pathways in pre- and post-synaptic neurons. This complex process involves multiple specializations in both pre- and post-synaptic compartments. In pre-synaptic neurons, these specializations include the formation of active zones, vesicle clustering, the synthesis and release of neurotransmitters, and the synaptic enrichment of mitochondria (Lee and Peng, 2008; Tang and Zucker, 1997; Brodin et al., 1999; Blaustein et al., 1978). In post-synaptic neurons, post-synaptic densities and clustering of neurotransmitter receptors occur (Sheng and Kim, 2011; Sheng, 2001).

Several studies have shown that retrograde signaling from the post-synaptic neuron modulates pre-synaptic signaling (Williams, 1996; Sastry et al., 1988). However, the mechanisms that maintain functional synaptic connections are poorly understood. To address this, we focused on mechanisms that regulate the synaptic availability of mitochondria because they are critical for synapse formation and function (Guo et al., 2005; Stowers et al., 2002; Morris and Hollenbeck, 1993; Misgeld and Schwarz, 2017; Lin and Sheng, 2015; MacAskill and Kittler, 2010; Saxton and Hollenbeck, 2012; Sheng and Cai, 2012; Cai and Tammineni, 2017).

We considered the possibility that the post-synaptic neurons continuously send signals to the pre-synaptic neurons to ensure the availability of mitochondria at the pre-synapse. Hence, we studied the active transport of mitochondria by kinesin-1 and dynein in the presence and absence of a functional synapse (Hirokawa et al., 1991; Glater et al., 2006; Schwarz, 2013; Varadi et al., 2004).

To study transport, we used the advantages of identified pre-synaptic and post-synaptic neurons in the sea slug *Aplysia californica*. Unlike vertebrate neurons that form autapses, *Aplysia* sensory neurons (SNs) and motor neurons (MNs) only form synapses between specific types of neurons (Kandel, 2001; Bailey et al., 2015; Glanzman, 2006; Hawkins et al., 2006). In the presence of L7MN, a target post-synaptic MN in the abdominal ganglia, SNs form glutamatergic synapses. However, when SNs are cultured with L11MN, only fasciculation occurs (Lyles et al., 2006). By culturing SNs with either L7MN or L11MN, questions about the specific effect of synapse formation can be addressed. Furthermore, because these neurons are large, SNs or MNs could be independently manipulated with high precision.

By comparing transport in SNs either grown alone or with a target or non-target MN, we find that synapse formation results in a persistent enhancement in bi-directional mitochondrial flux in pre-synaptic neurons. This is coupled with a persistent alteration in the pre-synaptic transcriptome. Once the synapses are formed, the inhibition of signaling from the post-synaptic neuron does not alter persistent enhancement in transport. However, inhibition of pre-synaptic transcription or protein synthesis blocks the enhancement in transport.

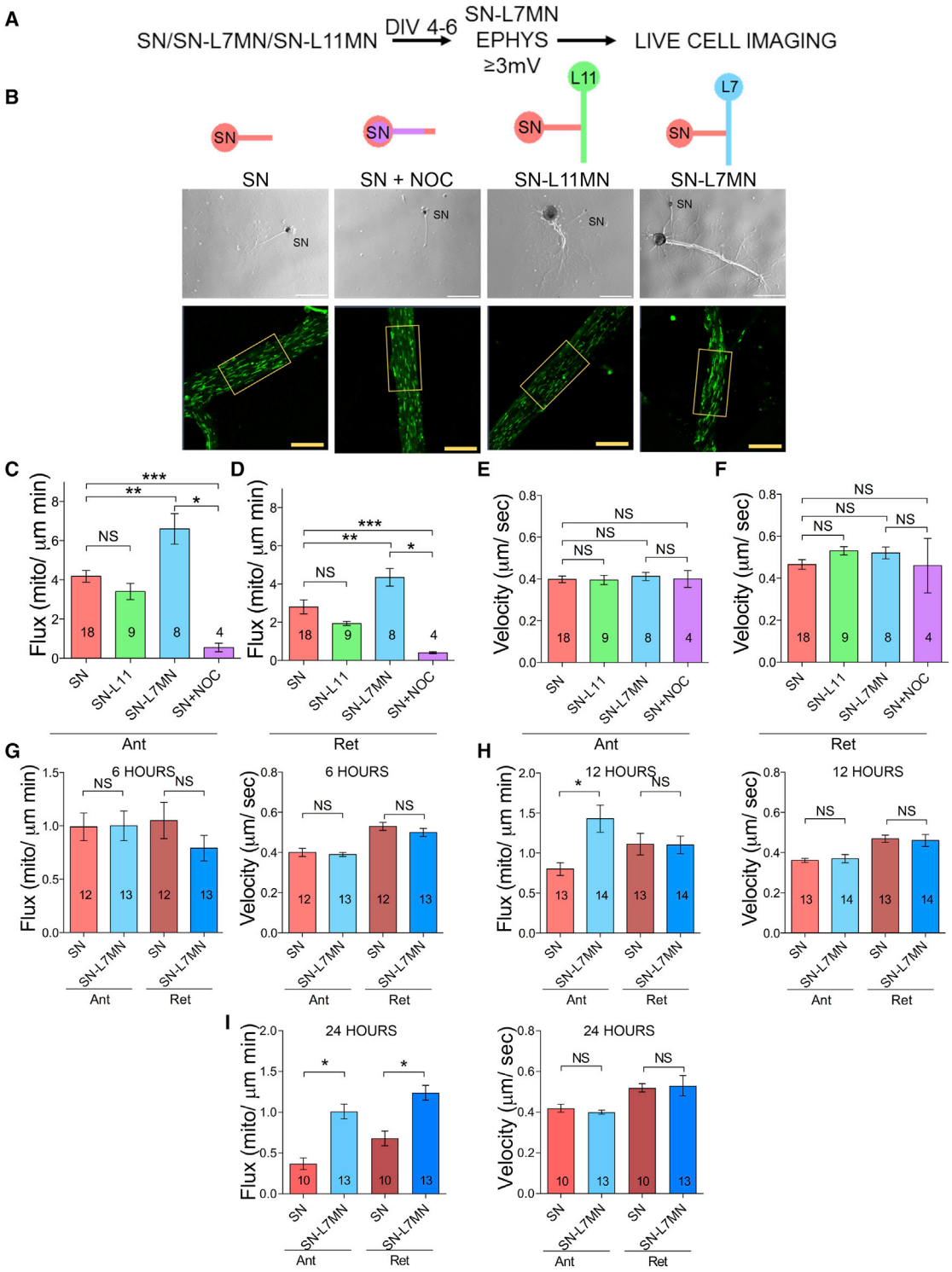

Figure 1. Synapse Formation Produces Persistently Enhanced Bi-directional Mitochondrial Transport in Pre-synaptic Sensory Neurons

(A) Experimental design.

(B) DIC and fluorescence images are shown. The fluorescence images in boxes show examples of a region where transport was analyzed. MN, motor neuron; NOC, nocodazole; SN, sensory neuron. Scale bar, 10 µm.

(legend continued on next page)

RESULTS

Synapse Formation Persistently Enhances Anterograde and Retrograde Mitochondrial Flux in Sensory Neurons

To assess whether mitochondrial transport is regulated for maintaining synaptic connections, we imaged MitoTracker-labeled mitochondria in days *in vitro* (DIV) 4–6 SNs and SN-MN cocultures (Figures 1A and 1B). We studied two parameters of transport: flux (*J*) (mitochondria/μm/min), which assesses the number of mitochondria that pass through a line across the axon over time, and velocity (*u*) (μm/s) (Figures S1A–S1C). These are related by the equation $J = \rho u$, where ρ is the density of moving mitochondria in units of mitochondria per square micron. First, we optimized the conditions for measurements in isolated single SNs and assessed the effect of nocodazole, an inhibitor of microtubule polymerization, on bi-directional mitochondrial transport. Consistent with previous studies, nocodazole (5 μM for 30 min) significantly decreased bi-directional flux, but it had no effect on the velocity of the few mitochondria that remained in motion (Figures 1C–1F; Table S1A).

Second, we compared transport in DIV 4–6 single SNs and SNs co-cultured with L7 MN (hereafter SN-L7MN). Synapses between these neurons form soon after plating, become mature within 3 days, and can be maintained up to 8–10 days in culture. We confirmed the presence of functional synapses by measuring excitatory post-synaptic potentials (EPSPs) using sharp electrodes. We only used cultures with EPSPs $\geq$3 mV for the time-lapse imaging experiments (Figures S1D–S1F).

Transport analysis indicated a significant increase in anterograde and retrograde flux in SNs when co-cultured with L7MN, compared to SNs grown alone, without a significant change in transport velocity (Figures 1C–1F; Table S1A). Representative images of transport in SN, SN-L7MN, and SN-L11 are shown in Video S1. Because flux is equal to velocity multiplied by the density of material in motion, these results suggest that synapse formation results in a robust and long-term increase in the number of mitochondria in motion in both anterograde and retrograde directions.

To test whether increased transport resulted from synapse formation or the effect of co-culture, we next grew SNs with the non-target motor neuron L11 MN (SN-L11MN) and assessed transport. We found no significant change in the flux or the velocity of mitochondrial transport (Figures 1C–1F; Table S1A). These data suggest that synapse formation increases bi-directional mitochondrial transport in a persistent manner by increasing the number of mitochondria in motion.

To better understand how mitochondrial transport changes during the process of synapse formation, we analyzed mitochondrial motion over time in individual SNs and SNs co-cultured with L7MNs. At 6 h, there were no effects, but by 12 h, anterograde flux significantly rose. Both anterograde and retrograde transport were significantly enhanced at 24 h as seen in DIV 4–6 cultures. Throughout the time course, there were no significant effects on velocity (Figures 1G–1I; Table S1A).

To determine whether this persistent increase in transport is specific to mitochondria, we conducted time-lapse differential interference contrast (DIC) imaging of vesicles in DIV 4–6 SNs and SN-L7MNs. Similar to mitochondria, there was a significant increase in anterograde flux but no change in retrograde flux in SN-L7MNs compared to SNs (Figures S1G–S1I; Table S1E). To further understand the regulation of organelle transport, we next imaged the transport of lysosomes in DIV 4–6 SNs and SN-L7MNs using LysoTracker. In contrast, retrograde flux significantly decreased in SN-L7MNs (Figures S1G, S1J, and S1K; Table S1E). This suggests that while there is a global increase in anterograde transport, specific organelles are independently regulated.

cAMP Signaling Is Necessary and Sufficient to Enhance the Flux of Bi-directional Mitochondrial Transport in Single Sensory Neurons

We next investigated the signaling pathways that regulate transport, with a focus on three that are critical for synaptic plasticity: inositol triphosphate (IP3) (Shuai et al., 2007; Swatton and Taylor, 2002), protein kinase C (PKC) (Furukawa et al., 1995; Kempsell and Fieber, 2015), and cyclic AMP (cAMP) (Azhderian et al., 1994). Our method was to expose SNs to either ADA (adenophostin A, activator of IP3 receptor signaling, concentration 10 μM) for 10 min, PMA (phorbol 12-myristate 13-acetate, activator of PKC signaling, concentration 50 nM) for 15 min, or forskolin (FK) (activator of cAMP signaling, concentration 50 μM) for 30 min. This was followed by analysis of mitochondrial transport. Consistent with reports that increased Ca^{2+} reduces anterograde mitochondrial transport (Rintoul et al., 2003; Yi et al., 2004; Hsin et al., 2006), exposure with ADA reduced anterograde mitochondrial flux. In contrast, PMA had no effects (Figures 2A–2C; Table S1B). However, FK enhanced anterograde flux in SNs, but it did not alter retrograde transport flux or velocity (Figures 2D–2G; Table S1B).

These results suggested a critical role for cAMP signaling in the persistent increase in mitochondrial flux following synapse formation. To further understand this, we assessed whether the activation of cAMP signaling may further enhance mitochondrial transport in SNs when co-cultured with L7MN. However, forskolin exposure did not increase the flux in SN-L7MNs (Figures 2D and 2E; Table S1B). This lack of an effect suggests that forskolin-induced changes in cAMP signaling could not produce further enhancements to those already produced by synapse formation. However, consistent with a role for cAMP in the regulation of transport, the protein kinase A (PKA) inhibitor 14-22 amide decreased mitochondrial transport to a level similar to that seen in SNs, suggesting that PKA has a critical role in

(C–F) Bar graphs show the flux and velocity of anterograde (Ant) and retrograde (Ret) mitochondrial transport in SN measured by kymograph analysis. Error bars are SEMs. NS, nonsignificant, *p < 0.05; **p < 0.01; ***p < 0.001. One-way ANOVA and Tukey post hoc test.
(G–I) Bar graphs show the flux and velocity of anterograde and retrograde transport in SN compared to SN co-cultured with L7MN at 6, 12, and 24 h after plating, respectively. Numbers of neurons analyzed are indicated in the bar graphs. Error bars are SEMs. NS, nonsignificant; *p < 0.05. Student's unpaired t test.
See also Figure S1 and Table S1A.

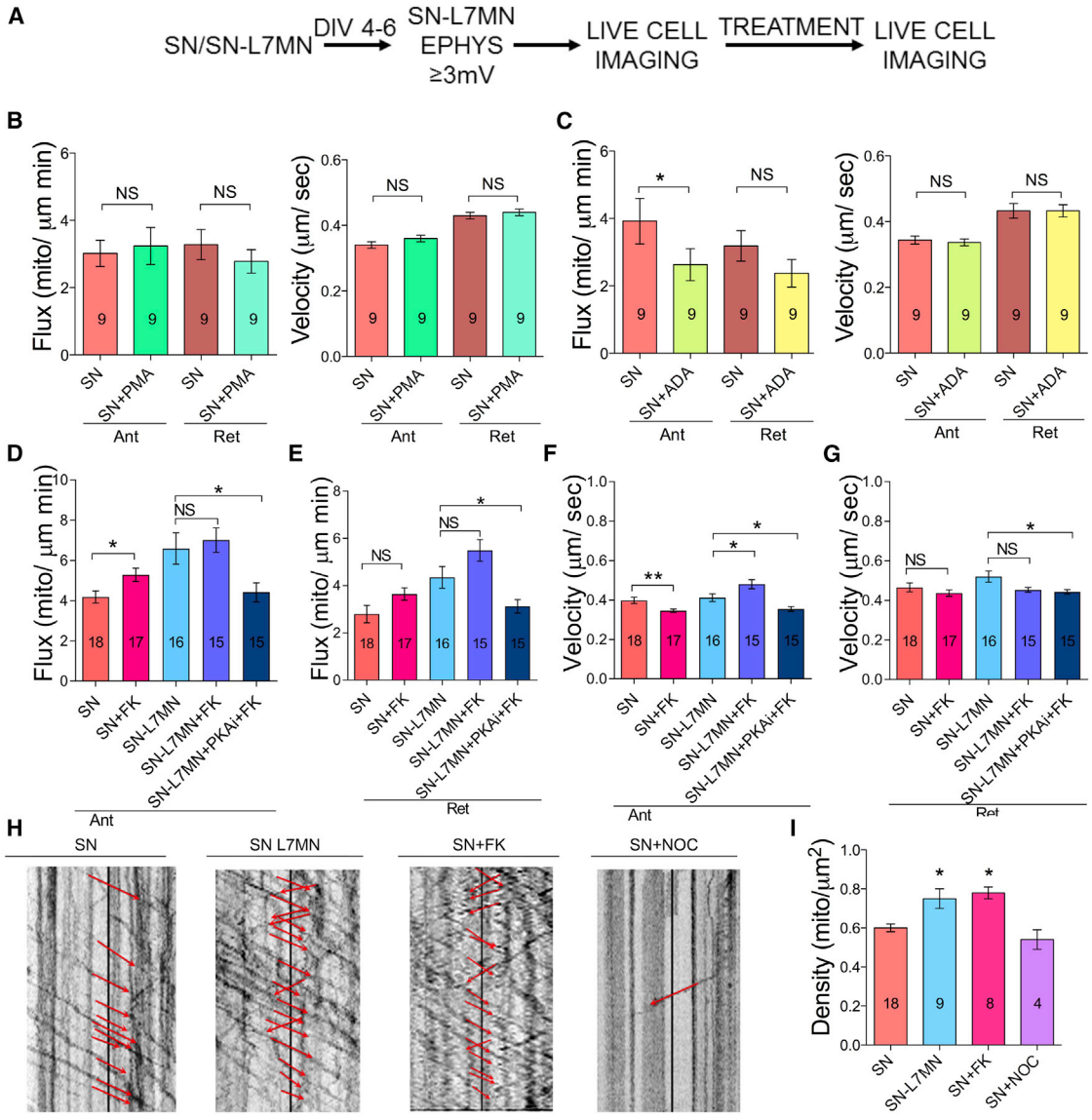

Figure 2. Activation of cAMP Signaling but Not IP3R Nor PKC Signaling Is Sufficient for Enhanced Mitochondrial Transport

(A) Experimental design.

(B–G) Bar graphs showing flux and velocity of anterograde and retrograde mitochondrial transport in SN measured in the presence of PMA, ADA, forskolin (FK), or FK+ PKAi (PKA inhibitor).

(H) Kymograph analysis following exposure to different pharmacological agents.

(I) Bar graph shows total mitochondrial density, which includes both stationary and transported mitochondria. The numbers of neurons analyzed are indicated in bar graphs.

Error bars are SEMs. NS, nonsignificant; *$p < 0.05$; ** $p < 0.05$. Student's unpaired t test. See also Figure S2 and Table S1B.

modulating the increase in transport associated with synapse formation (Figures 2D–2G; Table S1B).

We then examined how long the effect of forskolin in isolated SNs may last by studying mitochondrial transport 3 h after 30 min exposure of forskolin. While there were no changes in anterograde flux or velocity, we observed a significant increase in retrograde flux (Figures S2A and S2B; Table S1F). These results suggest that cAMP signaling is a key modulator of bi-directional mitochondrial transport.

Enhancement of Mitochondrial Transport Does Not Alter the Density of Stalled Mitochondria

The increase in the bi-directional transport of mitochondria associated with synapse formation could arise through increased biogenesis or an alteration in the balance between moving and docked mitochondria, or a combination of both. To distinguish between these possibilities, we measured the total density of mitochondria, as well as the density of mitochondria that were stationary and in motion in each direction. Comparing SN with

SN-L7MN, both total density and the density of anterogradely transported mitochondria increased significantly, but the concentration of stationary mitochondria did not increase significantly (Figures 2H, 2I, and 2C; Tables S1B S1F). This occurred without a significant decrease in the percentage of stationary mitochondria. This suggests that synapse formation primarily increases mitochondrial biogenesis, instead of mobilizing stationary mitochondria in the axon. Treatment with FK had similar effects in that it significantly increased the density of anterogradely transported mitochondria. Likewise, as expected, the inhibition of transport with nocodazole significantly decreased the density of transported mitochondria and increased the density of stationary mitochondria without having a significant effect on the total density. These results suggest that synapse formation persistently enhances mitochondrial transport by increasing the production of new mitochondria.

Inhibition of NMDA and AMPA Receptor Activity Does Not Alter the Enhanced Mitochondrial Flux in Pre-synaptic Neurons

We next asked how the post-synaptic neuron persistently enhances mitochondrial transport in pre-synaptic neurons. We focused on α-amino-3-hydroxy-5-methyl-4-isoxazolepropionic acid (AMPA) and *N*-methyl-D-aspartate (NMDA) receptor-mediated signaling, the two key post-synaptic signaling pathways that mediate glutamatergic synaptic transmission and plasticity (Dale and Kandel, 1993; Armitage and Siegelbaum, 1998; Ezzeddine and Glanzman, 2003). We first studied the effects of NMDA and AMPA receptor antagonists in synaptic transmission in SN-L7MN. Consistent with the necessity of these receptors in synaptic transmission, EPSP measurements in the presence of (DL)-2-amino-5-phosphonovaleric acid (APV) or cyanquixaline (CNQX) showed a significant reduction (Figures 3A–3C; Table S1C).

We next used these inhibitors in SN-L7MN cultures in the live cell imaging and transport measurements. Contrary to our expectations, we found that the inhibition of either NMDA or AMPA receptors at different time points (15 min, 30 min, 1 h, and 24 h) had no effect on mitochondrial flux or velocity (Figures 3D–3I; Table S1C). These results show that NMDA and AMPA receptor signaling does not contribute to persistently enhanced pre-synaptic mitochondrial transport. We found an increase in the flux of anterograde transport within 1 h of treatment, although at a later time point (24 h), there was no significant effect on flux or velocity.

Removal of the Cell Body of the Post-synaptic Motor Neuron Does Not Alter Enhanced Mitochondrial Flux in Pre-synaptic Neurons

To further test the contribution of the post-synaptic neuron in enhancing pre-synaptic transport, we examined whether signals generated in the L7MN cell body continuously modify pre-synaptic terminals for persistent enhancement in mitochondrial transport in SNs. A decrease in pre-synaptic mitochondrial transport with microdissection of L7MN would suggest the existence of a cell body-generated signal in modulating pre-synaptic transport. Hence, following basal EPSP recordings, we removed the L7MN cell body by microdissection and then measured bi-directional transport in SNs.

For these experiments, 24 or 72 h after the removal of the L7MN cell body, we measured mitochondrial transport in SNs. Quantitative transport analysis suggested that there were no significant effects on flux or velocity, as compared to pre-synaptic transport in the presence of intact post-synaptic cell body at either time point (Figures 4A–4D; Table S1D). These results argue against a signal generated by the post-synaptic cell body that enhances pre-synaptic mitochondrial transport in SNs.

Enhancement in Bi-directional Flux of Mitochondria Is Dependent on Transcription and Translation in Pre-synaptic Neurons

We next considered the possibility that synapse formation produces robust and long-term changes in the transcriptional program of the pre-synaptic neuron, resulting in enhanced mitochondrial transport. To test this, we used SN-L7MN with a microdissected L7MN cell body (to avoid the contribution of post-synaptic gene expression), as described earlier, and imaged mitochondrial transport following the inhibition of pre-synaptic transcription using the transcriptional inhibitor actinomycin D (50 μM for 2 h) 22 h after L7MN cell body dissection. A decrease in transport when compared to vehicle-treated controls would suggest the dependence on active transcription for persistently enhanced bi-directional mitochondrial transport.

The analysis suggested a decrease in the anterograde but not in the retrograde flux of mitochondria with no changes in velocity (Figure 4E; Table S1D). A representative video of mitochondrial transport following actinomycin exposure is shown in Video S2. These results indicate that changes in the pre-synaptic transcriptional program underlie the persistent enhancement in pre-synaptic mitochondrial transport that follows synapse formation.

Because transcription regulates the proteome, we tested whether enhanced mitochondrial transport depends on changes in protein synthesis. To assess this, we used the translation inhibitor anisomycin (10 μM for 24 h) following L7MN cell body dissection, as described above. Consistent with the transcriptional data, there were significant decreases in bi-directional mitochondrial flux and a reduction in the velocity of anterograde transport (Figure 4F; Table S1D; Video S3). These results corroborate that synapse formation produces persistent changes in transcription and translation in pre-synaptic neurons that result in enhanced pre-synaptic mitochondrial transport.

To understand whether translation is critical for the transport of other organelles, we assessed lysosomal transport in SN (in SN-L7MN cell body removed). An analysis of video data suggested that the inhibition of translation did not produce a deficit in anterograde or retrograde transport (Figure S3; Table S1G). This indicates differential requirements of translation in modulating organelle transport.

Synapse Formation Persistently Alters the Transcriptional Program of Pre-synaptic Neurons

To understand the changes in transcription driven by synapse formation, we identified transcripts that are differentially expressed in SNs in the presence of the post-synaptic neuron L7 (SN-L7MN) 4–6 days after synapse formation. Following electrophysiological validation of a functional synapse, SN cell bodies were microdissected from isolated SNs or SNs co-cultured

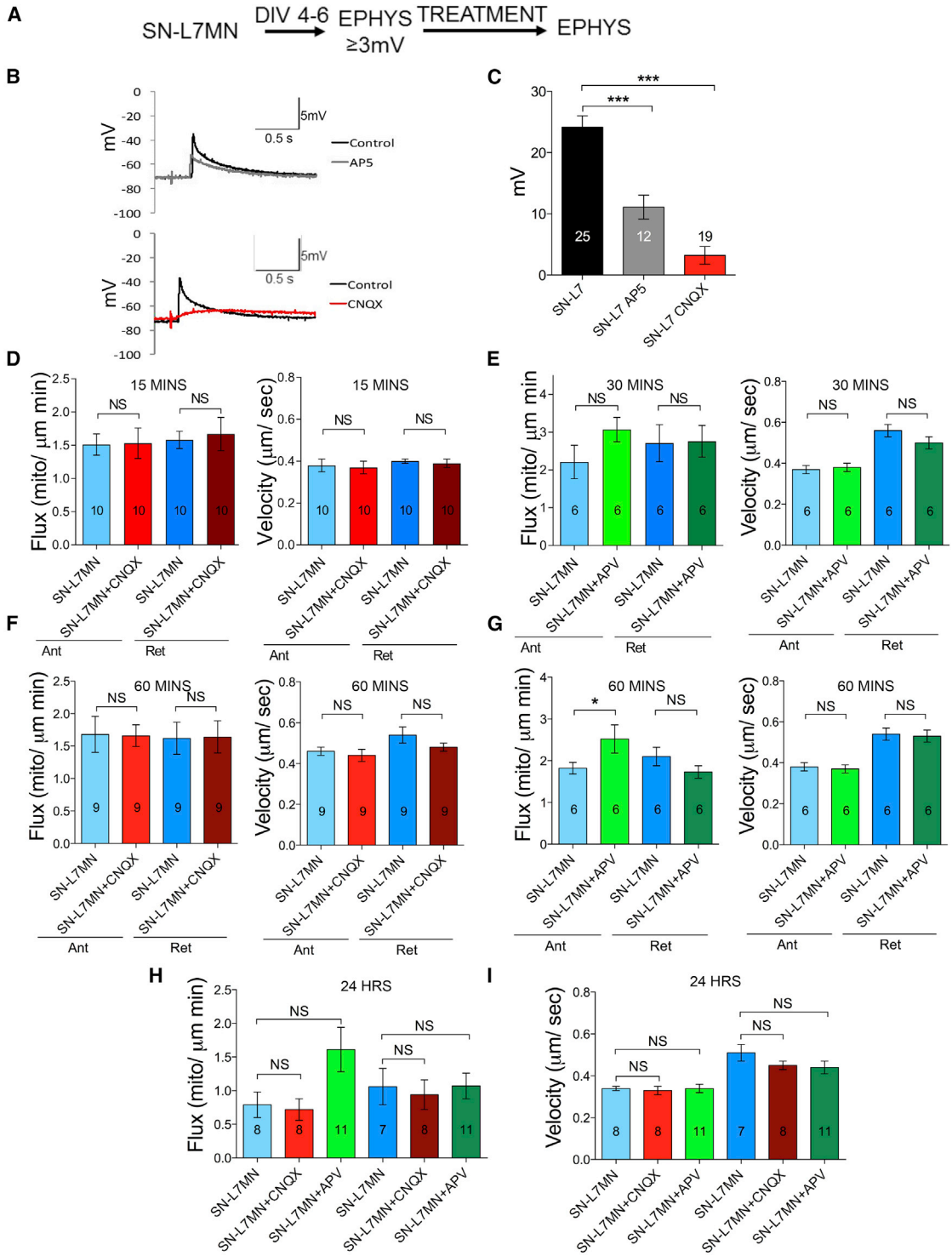

Figure 3. Role of NMDA and AMPA Receptor Signaling in Modulating Pre-synaptic Mitochondrial Transport

(A) Experimental design.

(B) Representative traces of 2 s recording before and after CNQX or APV.

(C) Bar graphs showing the quantitation of data in (B).

(D–I) Bar graphs showing the quantitation of flux and velocity of anterograde and retrograde transport at different time points: (D) 15 min CNQX; (E) 30 min APV; (F) 1 h CNQX; (G) 1 h APV; (H) 24 h CNQX and APV flux; (I) 24 h CNQX and APV velocity. The numbers of neurons used in the experiment are indicated in the bar graphs. Error bars are SEMs. NS, nonsignificant; *p < 0.05; ***p < 0.001. Student's unpaired t test. See also Table S1C.

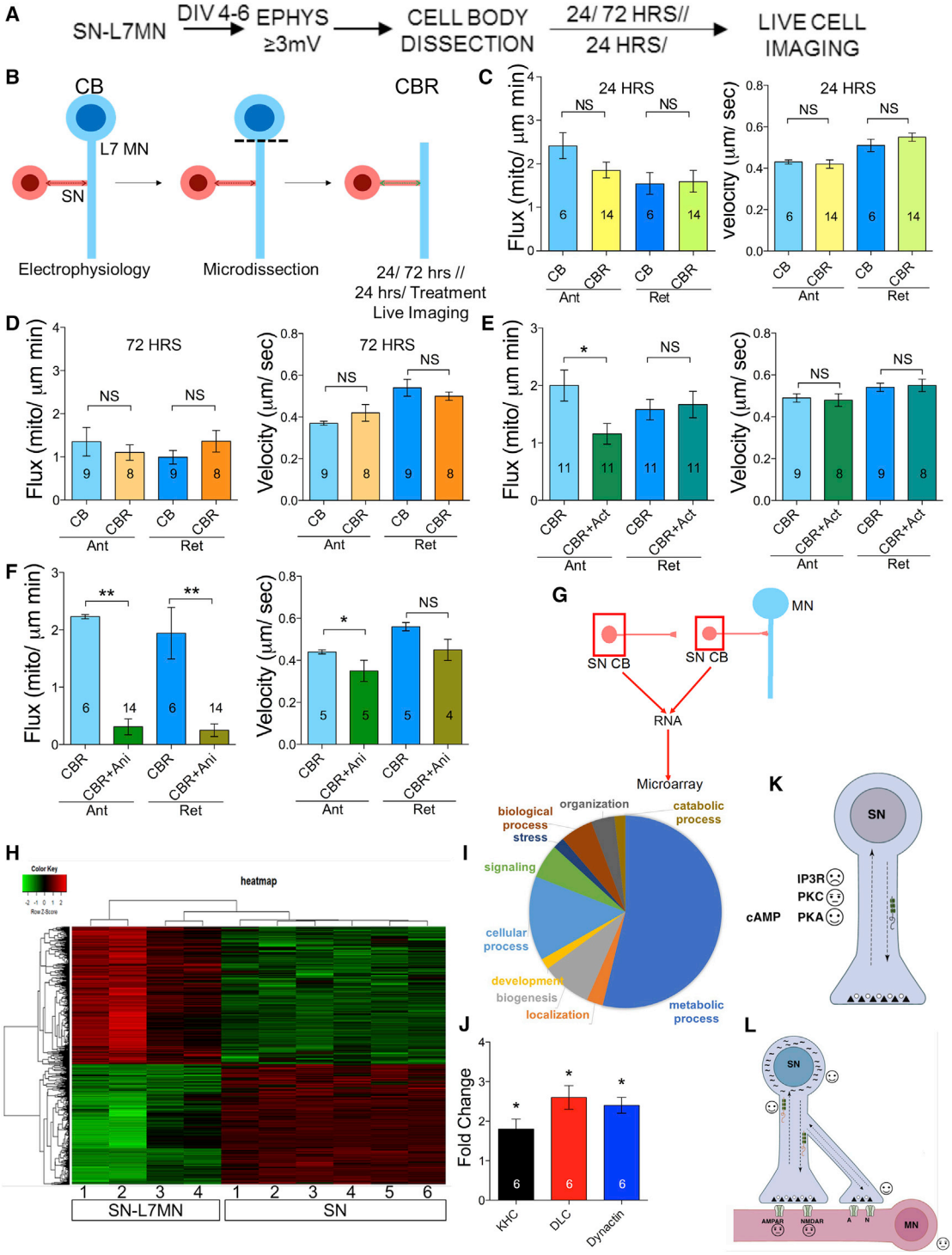

Figure 4. Role of Post-synaptic Neurons in Modulating Pre-synaptic Mitochondrial Transport

(A) Experimental design.

(B–F) Schematic of SN-L7MN microdissection. CB, L7MN with intact cell body. CBR, L7MN with cell body removed. Bar graphs show the measurements of the flux and velocity of anterograde and retrograde transport. Mitochondrial imaging was done on the SN 24 h or 72 h after removal of the L7MN cell body (C and D, respectively) and following exposure to (E) actinomycin D (Act) or (F) anisomycin (Ani). Numbers of neurons used in the experiment are indicated in the bar graphs. Error bars are SEMs. NS, nonsignificant; *p < 0.05; **p < 0.01. Student's unpaired t test.

(legend continued on next page)

with L7MN (Figures 4G, 4H, and S1D) and analyzed using an *Aplysia* microarray (Puthanveettil et al., 2013).

We identified ~4,000 differentially expressed mRNAs (>2-fold change, false discovery rate [FDR] ≤0.05) (Table S1H and S1I). Among these, 1,245 transcripts were successfully blasted against the RefSeq database (E value <10) using Blast2GO. Analysis of the microarray data by Gene Ontology (GO) revealed substantial changes corresponding to metabolism (~50% of differentially expressed genes) (Figure 4I), suggesting that elevated metabolism in SN is critical for maintaining neural circuit function.

Among the differentially expressed genes, we searched for known regulators of mitochondrial transport, including Miro (Cai and Sheng, 2009; Shlevkov et al., 2016), Milton (Stowers et al., 2002; Glater et al., 2006), and syntaphilin (Lin et al., 2017), as well as components of anterograde and retrograde transport. We found that critical components of anterograde transport machinery (kinesin-1 heavy chain [KHC]) and retrograde machinery (dynein light chain [DLC] and dynactin) were significantly elevated in SN-L7MN and were then validated by qPCR (Figure 4J). We then examined whether known genes involved in mitochondrial biogenesis such as PGC-1, PPAR, AMPK, CaMK IV, sirtulin 1, TORC, Sin3A, and p38MPAK (Jornayvaz and Shulman, 2010; Scarpulla et al., 2012) were among the differentially expressed genes. We found TORC 1 and PPAR mRNAs that are significantly upregulated in SNs (1.5- and 2.6-fold upregulation, respectively; Table S1K), suggesting that the expression of critical genes involved in mitochondrial biogenesis is persistently upregulated following synapse formation.

DISCUSSION

Persistent Changes in Pre-synaptic Mitochondrial Transport

Little is known about how intercellular signaling modulates the long-term changes in the components of neural circuitry that occur during synapse formation. To address this challenge, we assessed how post-synaptic neurons modulate transport in pre-synaptic neurons. We found that when a pre-synaptic neuron is co-cultured with the target post-synaptic motor neuron, bi-directional transport is enhanced in the pre-synaptic neuron (Figure 1A–1I). Because all of our measurements were carried out using mature synapses (DIV 4–6 cultures, synapses begin to form within day 1 of co-culture), this observation is intriguing. We assumed that synapse formation is an energy-demanding process and that enhanced mitochondrial transport is activated to meet the high-energy requirements. This raised the question why does mitochondrial transport need to be persistently enhanced upon synapse formation?

A possibility is that continuously maintaining proper synapse function requires substantial energy, and hence enhanced mitochondrial transport ensures the proper maintenance of synapse function. Consistent with this idea, Zhu et al. (2012) have shown that resting cortical neurons require 4.7 billion ATP molecules per second. Likewise, disruption of mitochondrial trafficking impairs synaptic function (Sheng and Cai, 2012). Since synaptic transmission does not occur in isolated pre-synaptic SNs (these neurons do not form autapses) or when SNs are grown with a non-target L11MN (Figure 1B), the energy requirements are lower. These results suggest that persistent enhancement in mitochondrial transport following synapse formation is a response to increased metabolic demands.

We then asked whether the persistent increase in transport is specific to mitochondria or there is a global increase in the transport of all organelles. Time-lapse DIC imaging suggested an increase in anterograde flux without a change in the retrograde flux (Figures S1G–S1I). However, imaging of the transport of another organelle, the lysosome, indicated a decrease in retrograde transport without a change in anterograde transport (Figures S1J and S1K). These results suggest that organelle transport is regulated independently following synapse formation.

To understand the signaling mechanism underlying the enhanced mitochondrial transport in SN, we assumed that specific intracellular signaling pathways are activated upon synapse formation. To test whether these pathways are rate limiting in SNs, we asked whether the pharmacological activation of signaling pathways such as IP3, PKC, and cAMP that are critical for synaptic plasticity could alter mitochondrial transport in single SNs grown alone. We found that the activation of cAMP signaling, but not PKC or IP3 signaling, is sufficient to enhance mitochondrial transport in SNs, whereas the inhibition of PKA when functional synapses are present decreases mitochondrial transport (Figure 2). This supports the recent observation that cAMP signaling regulates mitochondrial transport in the wing neurons of adult *Drosophila* (Vagnoni and Bullock, 2018) and suggests that cAMP signaling may link synaptic function and mitochondrial motion.

Role of the Post-synaptic Neuron in Modulating Pre-synaptic Transport

To assess the role of the post-synaptic neuron, we used pharmacological inhibitors of AMPA and NMDA receptors and asked

(G) Schematics of the experiment for microarray analysis. SNCBs were isolated from SN grown alone or co-cultured with L7MN (DIV 4–6). SN CB, sensory neuron cell body.
(H) Heatmap showing differential gene expression (red, upregulated; green, downregulated; 2-fold cutoff; FDR <0.05) in SN co-cultured with L7MN (n = 4) or SN alone (n = 6).
(I) Pie chart representing microarray data showing pathways that are enriched upon synapse formation.
(J) Bar graph shows fold change in transcripts that are enriched with synapse formation within the pre-synaptic SN. Fold increase in KHC (kinesin heavy chain), DLC (dynein light chain), and dynactin. qPCR validation of three genes that we identified from microarray analysis. Bar graphs show normalized fold changes in gene expression in SN-L7MN compared to SN alone. 18srRNA expression was used to normalize data. Error bars are SEMs; *p < 0.05; Student's t test.
(K and L) Summary of findings. Persistently enhanced mitochondrial transport through changes in the pre-synaptic transcriptional program. Positive, negative, and neutral changes in mitochondrial transport identified from our studies are shown using emojis. Arrows, bi-directional transport; black squiggly lines, differentially expressed transcripts; red squiggly lines with beads, polyribosomes. SN, pre-synaptic sensory neuron; MN, post-synaptic motor neuron.
See also Figures S3 and S4 and Tables S1D and S1H–S1K.

whether inhibition of AMPA or NMDA signaling would alter flux or velocity of transport in pre-synaptic neurons. Contrary to our expectations, we found that neither the inhibition of AMPA nor NMDA receptors decreased the flux of mitochondrial transport at different time points (Figures 3A–3I), suggesting that synaptic transmission is not responsible for persistently enhanced mitochondrial transport.

We then considered the possibility that post-synaptic neurons send signals such as neurotrophins (Poo, 2001), arachidonic acid, nitric oxide (NO), or carbon monoxide (Tao and Poo, 2001) constitutively to pre-synaptic neurons to enhance mitochondrial transport. To test this, we carried out microdissection experiments to remove the L7MN cell body and assessed mitochondrial transport. If the post-synaptic cell body generated signals constitutively to instruct the pre-synaptic neuron to enhance mitochondrial transport, then we would expect a decrease in mitochondrial transport with the removal of the cell body. We found that cell body removal did not significantly alter pre-synaptic transport flux either at 24 or 72 h (Figures 4A–4D), which argues against the existence of constitutive instructions from post-synaptic neurons.

To further understand this, we focused on pre-synaptic neurons and considered the possibility that synapse formation persistently alters the pre-synaptic transcriptome to enhance transport. We removed the cell body of the post-synaptic neuron and incubated the cultures with the transcriptional inhibitor actinomycin D for 2 h. In support of the necessity of transcription for the persistent enhancements in mitochondrial transport, we observed a significant decrease in anterograde flux (Figure 4E), but no change in retrograde flux. These results suggest that critical components of anterograde transport require frequent replenishments through transcription.

We then assessed the necessity of translation by inhibiting it using anisomycin. We found that inhibition for 24 h after L7MN cell body microdissection produced a decrease in both the flux and the velocity of bi-directional transport in SN (Figure 4F), suggesting that protein synthesis is a rate-determining step regulating bi-directional mitochondrial transport. This suggests that the bi-directional transport of mitochondria is under the control of a constitutive transcriptional and translational program that is set by the formation of a functional synapse. We then asked whether persistent changes in organelle transport require translation by imaging the transport of lysosomes. Inhibition of translation did not significantly alter lysosomal transport, which suggests differential requirements of translation in modulating organelle transport (Figures S3A and S3B).

To identify the products of the altered transcriptional program in pre-synaptic neurons, we carried out microarray analyses. We found that the expression of ~4,000 genes is persistently changed upon synapse formation. Approximately 50% of the genes that changed were involved in metabolism (Figure 4I), which is consistent with the idea that maintaining neuronal connections is an energy-demanding process, and hence, enhancement of the supply of mitochondria is required for proper synapse function. Consistent with our finding that synapse formation causes large-scale changes in gene expression, it has been shown that active regulation of gene expression is associated with synapse formation and refinement (West and Greenberg, 2011).

In summary, we discovered that the post-synaptic neuron produces a robust and persistent change in the transcriptional program of the pre-synaptic neuron, resulting in the specific modulation of organelle transport (Figures 4K and 4L). A deeper understanding of how intercellular signaling produces persistent changes in the transcriptional program enabling distinct changes in bi-directional transport will provide insights into our understanding of the functioning of neuronal networks.

STAR★METHODS

Detailed methods are provided in the online version of this paper and include the following:

- KEY RESOURCES TABLE
- CONTACTS FOR REAGENT AND RESOURCE SHARING
- EXPERIMENTAL MODEL AND SUBJECT DETAILS
- METHOD DETAILS
  - *Aplysia* neuronal cultures
  - Intracellular electrophysiology measurements
  - Drug treatments
  - Live cell imaging of mitochondrial transport
  - Analysis of time-lapse image data
  - Mitochondrial density analysis
  - Microarray, bioinformatics analysis, and qPCR
- QUANTIFICATION AND STATISTICAL ANALYSIS
- DATA AND SOFTWARE AVAILABILITY

SUPPLEMENTAL INFORMATION

Supplemental Information includes four figures, one table, and three videos and can be found with this article online at https://doi.org/10.1016/j.celrep.2018.12.073.

ACKNOWLEDGMENTS

We gratefully acknowledge funding support from the NIH (5R01MH094607-05 and 5R21MH108929-02) and the NSF (award no. 1453799), which enabled us to carry out this work.

AUTHOR CONTRIBUTIONS

Conceptualization, S.V.P.; Methodology, K.K.B., K.A., P.L., X.-A.L., S.S., K.E.M., and S.V.P.; Investigation, S.V.P., K.K.B., and K.E.M.; Data Analysis, K.E.M., K.K.B., M.-F.S., and A.R.; Writing & Editing, S.V.P., K.E.M., and K.K.B.; Overall Supervision, S.V.P.; Imaging Supervision, K.E.M.

DECLARATION OF INTERESTS

The authors declare no competing interests.

Received: May 27, 2018
Revised: November 18, 2018
Accepted: December 17, 2018
Published: January 15, 2019

REFERENCES

Armitage, B.A., and Siegelbaum, S.A. (1998). Presynaptic induction and expression of homosynaptic depression at Aplysia sensorimotor neuron synapses. J. Neurosci. *18*, 8770–8779.

Azhderian, E.M., Hefner, D., Lin, C.-H., Kaczmarek, L.K., and Forscher, P. (1994). Cyclic AMP modulates fast axonal transport in Aplysia bag cell neurons by increasing the probability of single organelle movement. Neuron *12*, 1223–1233.

Bailey, C.H., Kandel, E.R., and Harris, K.M. (2015). Structural Components of Synaptic Plasticity and Memory Consolidation. Cold Spring Harb. Perspect. Biol. *7*, a021758.

Baqri, R.M., Turner, B.A., Rheuben, M.B., Hammond, B.D., Kaguni, L.S., and Miller, K.E. (2009). Disruption of mitochondrial DNA replication in Drosophila increases mitochondrial fast axonal transport in vivo. PLoS One *4*, e7874.

Blaustein, M.P., Ratzlaff, R.W., and Kendrick, N.K. (1978). The regulation of intracellular calcium in presynaptic nerve terminals. Ann. N Y Acad. Sci. *307*, 195–212.

Brodin, L., Bakeeva, L., and Shupliakov, O. (1999). Presynaptic mitochondria and the temporal pattern of neurotransmitter release. Philos. Trans. R. Soc. Lond. B Biol. Sci. *354*, 365–372.

Cai, Q., and Sheng, Z.-H. (2009). Molecular motors and synaptic assembly. Neuroscientist *15*, 78–89.

Cai, Q., and Tammineni, P. (2017). Mitochondrial Aspects of Synaptic Dysfunction in Alzheimer's Disease. J. Alzheimers Dis. *57*, 1087–1103.

Dale, N., and Kandel, E.R. (1993). L-glutamate may be the fast excitatory transmitter of Aplysia sensory neurons. Proc. Natl. Acad. Sci. USA *90*, 7163–7167.

Ezzeddine, Y., and Glanzman, D.L. (2003). Prolonged habituation of the gill-withdrawal reflex in Aplysia depends on protein synthesis, protein phosphatase activity, and postsynaptic glutamate receptors. J. Neurosci. *23*, 9585–9594.

Furukawa, Y., Kim, H.N., and Kubo, T. (1995). Up- and down-modulation of a cloned Aplysia K+ channel (AKv1.1a) by the activators of protein kinase C. Zool. Sci. *12*, 35–44.

Gentleman, R.C., Carey, V.J., Bates, D.M., Bolstad, B., Dettling, M., Dudoit, S., Ellis, B., Gautier, L., Ge, Y., Gentry, J., et al. (2004). Bioconductor: open software development for computational biology and bioinformatics. Genome Biol. *5*, R80.

Glanzman, D.L. (2006). The cellular mechanisms of learning in Aplysia: of blind men and elephants. Biol. Bull. *210*, 271–279.

Glater, E.E., Megeath, L.J., Stowers, R.S., and Schwarz, T.L. (2006). Axonal transport of mitochondria requires milton to recruit kinesin heavy chain and is light chain independent. J. Cell Biol. *173*, 545–557.

Guo, X., Macleod, G.T., Wellington, A., Hu, F., Panchumarthi, S., Schoenfield, M., Marin, L., Charlton, M.P., Atwood, H.L., and Zinsmaier, K.E. (2005). The GTPase dMiro is required for axonal transport of mitochondria to Drosophila synapses. Neuron *47*, 379–393.

Hawkins, R.D., Kandel, E.R., and Bailey, C.H. (2006). Molecular mechanisms of memory storage in Aplysia. Biol. Bull. *210*, 174–191.

Hirokawa, N., Sato-Yoshitake, R., Kobayashi, N., Pfister, K.K., Bloom, G.S., and Brady, S.T. (1991). Kinesin associates with anterogradely transported membranous organelles in vivo. J. Cell Biol. *114*, 295–302.

Hsin, Y.-H., Cheng, C.-H., Tzen, J.T.C., Wu, M.-J., Shu, K.-H., and Chen, H.-C. (2006). Effect of aristolochic acid on intracellular calcium concentration and its links with apoptosis in renal tubular cells. Apoptosis *11*, 2167–2177.

Jornayvaz, F.R., and Shulman, G.I. (2010). Regulation of mitochondrial biogenesis. Essays Biochem. *47*, 69–84.

Kadakkuzha, B.M., Akhmedov, K., Capo, T.R., Carvalloza, A.C., Fallahi, M., and Puthanveettil, S.V. (2013). Age-associated bidirectional modulation of gene expression in single identified R15 neuron of Aplysia. BMC Genomics *14*, 880.

Kandel, E.R. (2001). The molecular biology of memory storage: a dialogue between genes and synapses. Science *294*, 1030–1038.

Kempsell, A.T., and Fieber, L.A. (2015). Age-related deficits in synaptic plasticity rescued by activating PKA or PKC in sensory neurons of Aplysia californica. Front. Aging Neurosci. *7*, 173.

Lee, C.W., and Peng, H.B. (2008). The function of mitochondria in presynaptic development at the neuromuscular junction. Mol. Biol. Cell *19*, 150–158.

Lin, M.-Y., and Sheng, Z.-H. (2015). Regulation of mitochondrial transport in neurons. Exp. Cell Res. *334*, 35–44.

Lin, M.-Y., Cheng, X.-T., Xie, Y., Cai, Q., and Sheng, Z.-H. (2017). Removing dysfunctional mitochondria from axons independent of mitophagy under pathophysiological conditions. Autophagy *13*, 1792–1794.

Lyles, V., Zhao, Y., and Martin, K.C. (2006). Synapse formation and mRNA localization in cultured Aplysia neurons. Neuron *49*, 349–356.

MacAskill, A.F., and Kittler, J.T. (2010). Control of mitochondrial transport and localization in neurons. Trends Cell Biol. *20*, 102–112.

Martin, K.C., Casadio, A., Zhu, H., Yaping, E., Rose, J.C., Chen, M., Bailey, C.H., and Kandel, E.R. (1997). Synapse-specific, long-term facilitation of aplysia sensory to motor synapses: a function for local protein synthesis in memory storage. Cell *91*, 927–938.

Miller, K.E., and Sheetz, M.P. (2004). Axonal mitochondrial transport and potential are correlated. J. Cell Sci. *117*, 2791–2804.

Miller, K.E., DeProto, J., Kaufmann, N., Patel, B.N., Duckworth, A., and Van Vactor, D. (2005). Direct observation demonstrates that Liprin-α is required for trafficking of synaptic vesicles. Curr. Biol. *15*, 684–689.

Miniaci, M.C., Kim, J.-H., Puthanveettil, S.V., Si, K., Zhu, H., Kandel, E.R., and Bailey, C.H. (2008). Sustained CPEB-dependent local protein synthesis is required to stabilize synaptic growth for persistence of long-term facilitation in Aplysia. Neuron *59*, 1024–1036.

Misgeld, T., and Schwarz, T.L. (2017). Mitostasis in Neurons: Maintaining Mitochondria in an Extended Cellular Architecture. Neuron *96*, 651–666.

Montarolo, P.G., Goelet, P., Castellucci, V.F., Morgan, J., Kandel, E.R., and Schacher, S. (1986). A critical period for macromolecular synthesis in long-term heterosynaptic facilitation in Aplysia. Science *234*, 1249–1254.

Morris, R.L., and Hollenbeck, P.J. (1993). The regulation of bidirectional mitochondrial transport is coordinated with axonal outgrowth. J. Cell Sci. *104*, 917–927.

Poo, M.M. (2001). Neurotrophins as synaptic modulators. Nat. Rev. Neurosci. *2*, 24–32.

Puthanveettil, S.V., Antonov, I., Kalachikov, S., Rajasethupathy, P., Choi, Y.-B., Kohn, A.B., Citarella, M., Yu, F., Karl, K.A., Kinet, M., et al. (2013). A strategy to capture and characterize the synaptic transcriptome. Proc. Natl. Acad. Sci. USA *110*, 7464–7469.

Rintoul, G.L., Filiano, A.J., Brocard, J.B., Kress, G.J., and Reynolds, I.J. (2003). Glutamate decreases mitochondrial size and movement in primary forebrain neurons. J. Neurosci. *23*, 7881–7888.

Sastry, B.R., Goh, J.W., May, P.B.Y., and Chirwa, S.S. (1988). The involvement of nonspiking cells in long-term potentiation of synaptic transmission in the hippocampus. Can. J. Physiol. Pharmacol. *66*, 841–844.

Saxton, W.M., and Hollenbeck, P.J. (2012). The axonal transport of mitochondria. J. Cell Sci. *125*, 2095–2104.

Scarpulla, R.C., Vega, R.B., and Kelly, D.P. (2012). Transcriptional integration of mitochondrial biogenesis. Trends Endocrinol. Metab. *23*, 459–466.

Schwarz, T.L. (2013). Mitochondrial trafficking in neurons. Cold Spring Harb. Perspect. Biol. *5*, a011304.

Sheng, M. (2001). Molecular organization of the postsynaptic specialization. Proc. Natl. Acad. Sci. USA *98*, 7058–7061.

Sheng, Z.-H., and Cai, Q. (2012). Mitochondrial transport in neurons: impact on synaptic homeostasis and neurodegeneration. Nat. Rev. Neurosci. *13*, 77–93.

Sheng, M., and Kim, E. (2011). The postsynaptic organization of synapses. Cold Spring Harb. Perspect. Biol. *3*, a005678.

Shlevkov, E., Kramer, T., Schapansky, J., LaVoie, M.J., and Schwarz, T.L. (2016). Miro phosphorylation sites regulate Parkin recruitment and mitochondrial motility. Proc. Natl. Acad. Sci. USA *113*, E6097–E6106.

Shuai, J., Pearson, J.E., Foskett, J.K., Mak, D.-O.D., and Parker, I. (2007). A kinetic model of single and clustered IP3 receptors in the absence of Ca2+ feedback. Biophys. J. *93*, 1151–1162.

Smyth, G.K. (2004). Linear models and empirical bayes methods for assessing differential expression in microarray experiments. Stat. Appl. Genet. Mol. Biol. *3*, Article3.

Stowers, R.S., Megeath, L.J., Górska-Andrzejak, J., Meinertzhagen, I.A., and Schwarz, T.L. (2002). Axonal transport of mitochondria to synapses depends on milton, a novel Drosophila protein. Neuron *36*, 1063–1077.

Swatton, J.E., and Taylor, C.W. (2002). Fast biphasic regulation of type 3 inositol trisphosphate receptors by cytosolic calcium. J. Biol. Chem. *277*, 17571–17579.

Tang, Y., and Zucker, R.S. (1997). Mitochondrial involvement in post-tetanic potentiation of synaptic transmission. Neuron *18*, 483–491.

Tao, H.W., and Poo, M. (2001). Retrograde signaling at central synapses. Proc. Natl. Acad. Sci. USA *98*, 11009–11015.

Vagnoni, A., and Bullock, S.L. (2018). A cAMP/PKA/Kinesin-1 Axis Promotes the Axonal Transport of Mitochondria in Aging Drosophila Neurons. Curr. Biol. *28*, 1265–1272.e4.

Varadi, A., Johnson-Cadwell, L.I., Cirulli, V., Yoon, Y., Allan, V.J., and Rutter, G.A. (2004). Cytoplasmic dynein regulates the subcellular distribution of mitochondria by controlling the recruitment of the fission factor dynamin-related protein-1. J. Cell Sci. *117*, 4389–4400.

West, A.E., and Greenberg, M.E. (2011). Neuronal activity-regulated gene transcription in synapse development and cognitive function. Cold Spring Harb. Perspect. Biol. *3*, a005744.

Williams, J.H. (1996). Retrograde messengers and long-term potentiation: a progress report. J. Lipid Mediat. Cell Signal. *14*, 331–339.

Yi, M., Weaver, D., and Hajnóczky, G. (2004). Control of mitochondrial motility and distribution by the calcium signal: a homeostatic circuit. J. Cell Biol. *167*, 661–672.

Zhu, X.-H., Qiao, H., Du, F., Xiong, Q., Liu, X., Zhang, X., Ugurbil, K., and Chen, W. (2012). Quantitative imaging of energy expenditure in human brain. Neuroimage *60*, 2107–2117.

STAR★METHODS

KEY RESOURCES TABLE

REAGENT or RESOURCE	SOURCE	IDENTIFIER
Chemicals		
Nocodazole	Millipore Sigma	Cat#M1404
PKI 14-22 amide, myristoylated	Tocris, Bio-Techne	Cat#2546
Forskolin from *Coleus forskohlii*	Millipore Sigma	Cat#F6886
Adenophostin A, Hexasodium Salt	Millipore Sigma	Cat#115500
Phorbol 12-Myristate 13-Acetate	Millipore Sigma	Cat#19-144
D(-)-2-Amino-5-phosphonopentanoic acid (AP5)	Millipore Sigma	Cat#A8054
6-cyano-7-nitroquinoxaline-2,3-dione (CNQX)	Millipore Sigma	Cat#377406
Actinomycin D	Millipore Sigma	Cat#A1410
Anisomycin from *Streptomyces griseolus*	Millipore Sigma	Cat#A9789
MitoTracker Green FM	ThermoFisher Scientific	Cat#M7514
LysoTracker Deep Red	ThermoFisher Scientific	Cat#L12492
Dimethyl sulfoxide	Millipore Sigma	Cat#276855
L-15 Medium (Leibovitz)	Millipore Sigma	Cat#L5520
L-Glutamine Solution	Millipore Sigma	Cat#G7513
qScript cDNA Supermix	Quanta Biosciences	Cat# 101414-106
PowerUp SYBR Green Master Mix	Thermofisher	Cat# A2557
Data Availability		
Microarray Data	NCBI GEO	GPL24208
Experimental Methods: Organism		
Aplysia californica	University of Miami, Rosenstiel School, National resource for Aplysia	1-4grams
Aplysia californica	University of Miami, Rosenstiel School, National resource for Aplysia	80-120 g, 6months old
Software		
Prism 5 (version 5.0f)	GraphPad Software	https://www.graphpad.com/scientific-software/prism/
ImageJ	NIH	https://imagej.nih.gov/ij/
Minitab 18	Minitab Inc.	http://www.minitab.com/en-us

CONTACTS FOR REAGENT AND RESOURCE SHARING

Further information and requests for resources and reagents should be directed to and fulfilled by the Lead Contact, Sathyanarayanan Puthanveettil (sputhanv@scripps.edu).

EXPERIMENTAL MODEL AND SUBJECT DETAILS

Aplysia californica (2-6 months old) were obtained from the National *Aplysia* Resource Facility at the Rosenstiel School of Marine and Atmospheric Science, University of Miami and were housed in saltwater tanks on-site at Scripps Florida.

METHOD DETAILS

Aplysia neuronal cultures

Aplysia neuronal cultures were prepared as described previously (Montarolo et al. 1986). Briefly, abdominal ganglia from juvenile animals between 1 and 4 g of weight were isolated and processed for their motor neurons while the pleural ganglia of animals between 80 and 120 g of weight and 6 months of age were dissected and processed for their sensory neurons. The ganglia were digested in

modified L15 (Montarolo et al., 1986; Martin et al., 1997) and Dispase (GIBCO - 1680920). Ganglia were then washed in modified L15 and transferred to a dish containing 25% hemolymph (isolated from wild animals), 75% modified L15 and L-Glutamine (Sigma-Aldrich G7513). The ganglia were pinned down, and individual cells were removed and then plated in glass-bottom dishes with coverslips coated with poly-L-lysine. The media was composed of 25% hemolymph, modified L15 and L-Glutamine. L7 or L11 motor neurons (L7MN or L11 MN) were plated first then 30 mins after cells have adhered sensory neurons were plated with their axons overlaying the motor neuron axon. Single sensory neurons (SNs) were plated with their axons parallel to one another. Dishes containing the neuronal cultures were left overnight at room temperature then incubated at 17-18°C for four days before being used for experiments.

Intracellular electrophysiology measurements

Excitatory post-synaptic potentials (EPSPs) were measured as described previously (Miniaci et al., 2008; Martin et al., 1997). Briefly, the recording electrode was filled with 2.5M KCl and tested to ensure a resistance between 4-10 Mega Ohms. The stimulating electrode was coated with silver paint and filled with modified L15 media. A silver wire was wrapped around the stimulating electrode while another was placed inside the electrode. The L7MN cell body was impaled with the recording electrode and the presence of action potentials were used as an indication of health. To induce EPSPs, MNs were manually hyperpolarized and held at −85 millivolts (mV). The SNs were then stimulated with current lasting 2 ms and changes in the L7MN's membrane potential were measured. Sensory neurons that induced EPSPs of $\geq$ 3mV in the post-synaptic neurons were used for imaging, microarray, and qPCR analysis.

Drug treatments

To image fluorescently labeled mitochondria trafficking, cells were incubated with MitoTracker Green FM [300nM] dissolved in DMSO for 40 mins. To image fluorescently labeled lysosomes, cells were incubated with LysoTracker Deep Red [75 nM] dissolved in DMSO for 30 mins. The following pharmacological agents/vehicles were used to treat SN/SN-L7MNs: Nocodazole (NOC) [5 μM]/DMSO for 30 mins; Phorbol 12-Myristate 13-Acetate (PMA) [50nM]/DMSO for 15 mins; Adenophostin A (ADA) [10 μM]/water for 10 mins; Forskolin (FK) [50 μM]/DMSO for 30 mins; 14-22 Amide (PKAi) [360 nM]/water for 30 mins; D(-)-2-Amino-5-phosphonopentanoic acid (AP5) [100 μM] /water for 30 mins, 1 hr and 24 hr; 6-cyano-7-nitroquinoxaline-2,3-dione (CNQX) [50 μM]/water for 15 mins, 1 hr or 24 hr; Actinomycin D (Act) [50 μM] /DMSO for 2 hr and Anisomycin (Ani) [10 μM]/PBS for 2hrs.

Live cell imaging of mitochondrial transport

Neuronal cultures were treated with 300nM Mitotracker Green FM (ThermoFisher Scientific M7514) to fluorescently label mitochondria. To label lysosomes, cultures were treated with 75nM Lysotracker Deep Red (ThermoFisher Scientific L12492). Live imaging (regions that are 200 μm away from the cell body) videos are obtained using Zeiss 880 Confocal Microscope. Videos were acquired at 63x oil objective, at a timescale of 2.17 s with 200 cycles, therefore a recording duration of about 7.5 mins. Lysosomal tracking videos were at a timescale of 1.10 s with 250 cycles, and DIC videos were at a timescale of 370.9 ms with 600 cycles. The imaging field was 45.0 μm by 45.0 μm, and videos were saved as .czi files.

Analysis of time-lapse image data

To analyze mitochondrial transport, movies are rotated, cropped, and kymographs are constructed and analyzed in ImageJ as previously described (Miller and Sheetz, 2004; Miller et al., 2005; Baqri et al., 2009). Because *Aplysia* axons are several microns thick, the axon is divided into 1.3 μm sections, and each section is z-projected to create a stack of kymographs for each axon. To analyze flux and velocity, a line is drawn down the center of each kymograph. Lines are then traced over mitochondria that pass the center line, and the slope of each is recorded and exported to Excel. Flux is calculated as the sum of mitochondria that pass the center point in the anterograde and retrograde directions over time for the stack of kymographs, which is then divided by the width of the axon. Velocity for each direction is calculated based on the slopes. Averages, standard errors, and significance are calculated based on the data from individual neurons in Excel.

Mitochondrial density analysis

To measure the density of stationary mitochondria, two independent approaches are used. First, time lapse movies are median Z-projected in ImageJ. The number of mitochondria is counted and divided by the length and width of the axon to give an estimate in units of mitochondria / μm^2. This approach has the advantage of being straightforward but may underestimate density when mitochondria are close together. To address this, kymographs are constructed, and the number of stationary mitochondria is divided by the length and width of the region analyzed. The approach has the strength of resolving individual mitochondria that are close together but may lead to overestimates in density. In consideration of this bias, the results from the two approaches are averaged for each axon. The means are then exported to Minitab and analyzed by one-way ANOVA with Post hoc Fisher Pairwise comparison.

Microarray, bioinformatics analysis, and qPCR

Total RNAs were isolated from microdissected SN cell bodies of SNs or SN-L7MNs (DIV 4-6) using Trizol and purity and integrity were assessed using a RNA Nano chip (Agilent Technologies) using Eukaryote Total RNA Nano series protocol. The total RNA was subjected to two rounds of linear IVT-amplification and labeled with Cy3-labeled CTP using Amino Allyl MessageAmp II Amplification kits

(Invitrogen). 1.65 ug of labeled aRNA is hybridized on to microarrays (Agilent's 4x44k format arrays, Puthanveettil et al., 2013;, Kadakkuzha et al., 2013). The intensities of the scanned fluorescence images were extracted with Agilent Feature Extraction software version 10.7.3.1. The mean signals were background corrected and transformed to the log2 scale. The empirical Bayes moderated t-statistics, which is implemented in the limma Bioconductor package (Smyth, 2004), were used for differential expression detection. The Benjamini and Hochberg's approach was used to control for false discovery. Genes with at least 2-fold changes at the 95% confidence level were considered as being significantly different. The hierarchical clustering and other statistical analyses were performed using R/Bioconductor (Gentleman et al., 2004). This data have been deposited (GPL24208) in the Gene Expression Omnibus (GEO) database (https://www.ncbi.nlm.nih.gov/geo). Principal component analysis (PCA) was performed with Partek Genomics Suite (Partek Inc. St. Louis, MO). To ensure maximum accuracy for annotation of the signature list (5,158 microarray probes), the probes were blasted against the assembled RNA transcripts (www.aplysiagenetools.org). A BLAST database was prepared and a BLASTN was performed against this database using the flat file containing the microarray probes, resulting in 4,346 hits (E-value < 1).

Out of 4,346 transcripts, 1,245 were successfully blasted (tblastx) against the RefSeq database (E-value < 10) using the BLAST2GO application (https://www.blast2go.com). Mapping and annotation were performed based on default parameters in the BLATS2GO application. Additionally, InterProScan function was utilized to improve the gene ontology analysis results. GO analysis for upregulated and downregulated hits shown in the Table S1J was performed using GO-Slim and combined graph function in BLAST2GO. The sequence filter was set to 5.

Expression changes in KHC, DLC, and dynactin identified from microarray analysis were independently validated by qPCR (as described in Kadakkuzha et al., 2013).

QUANTIFICATION AND STATISTICAL ANALYSIS

P values were calculated in either Microsoft Excel or GraphPad Prism and derived using unpaired two-tailed Students' t test or one-Way ANOVA. Fisher or Tukey tests were used for post hoc analyses. Significance was defined as $p < 0.05$. The numbers of replications 'n'' and statistical tests used are described in each figure.

DATA AND SOFTWARE AVAILABILITY

All imaging and transcriptomics data described in this study are available upon request. The accession number for the microarray data reported in this paper is GPL24208.

Cell Reports, Volume *26*

Supplemental Information

Synapse Formation Activates a Transcriptional Program for Persistent Enhancement in the Bi-directional Transport of Mitochondria

Kerriann K. Badal, Komol Akhmedov, Phillip Lamoureux, Xin-An Liu, Adrian Reich, Mohammad Fallahi-Sichani, Supriya Swarnkar, Kyle E. Miller, and Sathyanarayanan V. Puthanveettil

Supplementary Figures

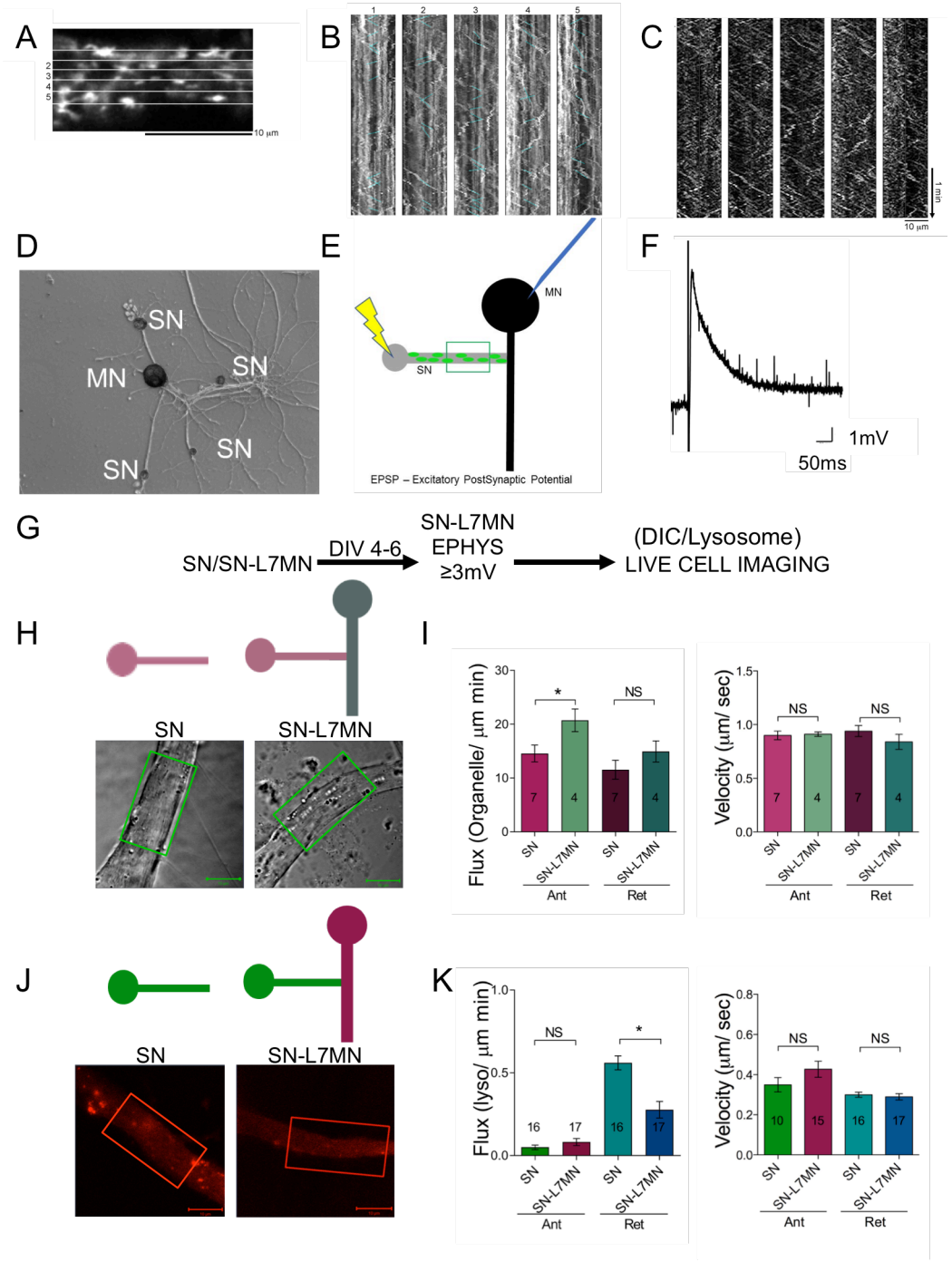

Supplementary Figure S1 Related to Figure 1. A: First frame of a time-lapse movie showing mitochondrial transport. The cell body is towards the left and the movie is split into 1.3 μm regions shown by the white horizontal lines (labeled 1 - 5). **B:** Each region is made into a kymograph. **C:** To enhance the visualization of transport through regions

where mitochondria are stationary, the movie is processed using a background subtraction algorithm and a second set of kymographs are constructed for reference. Lines, shown in light blue, are traced over mitochondria that clearly cross the center of the axon. Flux in each direction is calculated by counting the number of mitochondria that cross the center line and dividing by the time of the movie and width of the analyzed region (i.e. 1.3 μm). Velocity is calculated from the line slopes; bars = 10 μm, time arrow = 1 min. **D:** *Aplysia* neuronal cell culture with labeled MN (Motor neurons) and SNs (Sensory Neurons). **E:** Cartoon schematic of electrophysiology recording: EPSP – excitatory post-synaptic potential by stimulating SN and intracellular recording form MN. **F.** Trace of an EPSP recording from SN-L7MN co-culture. **G:** Experimental design schematic. **H.** Representative snapshots of transport in DIC live imaging in SN or SN-L7MN. Scale bar 10 μm. **I.** Bar graphs showing measurements of flux and velocity of anterograde (Ant) and retrograde (Ret) transport in SN or SN-L7MN. NS: non-significant. Error bars are SEM. "*" is $p < 0.05$; Student's t test. Numbers of neurons used indicated in bar graphs. **J.** Representative snapshots of transport in lysosome live imaging in SN or SN-L7MN. Scale bar 10 μm. **K.** Bar graphs showing measurements of flux and velocity of transport in SN or SN-L7MN. NS: non-significant. Error bars are SEM. Values are shown in Supplementary Table S5. Numbers of neurons used indicated in bar graphs "*" is $p < 0.05$; Student's unpaired t test. See also Table S1E.

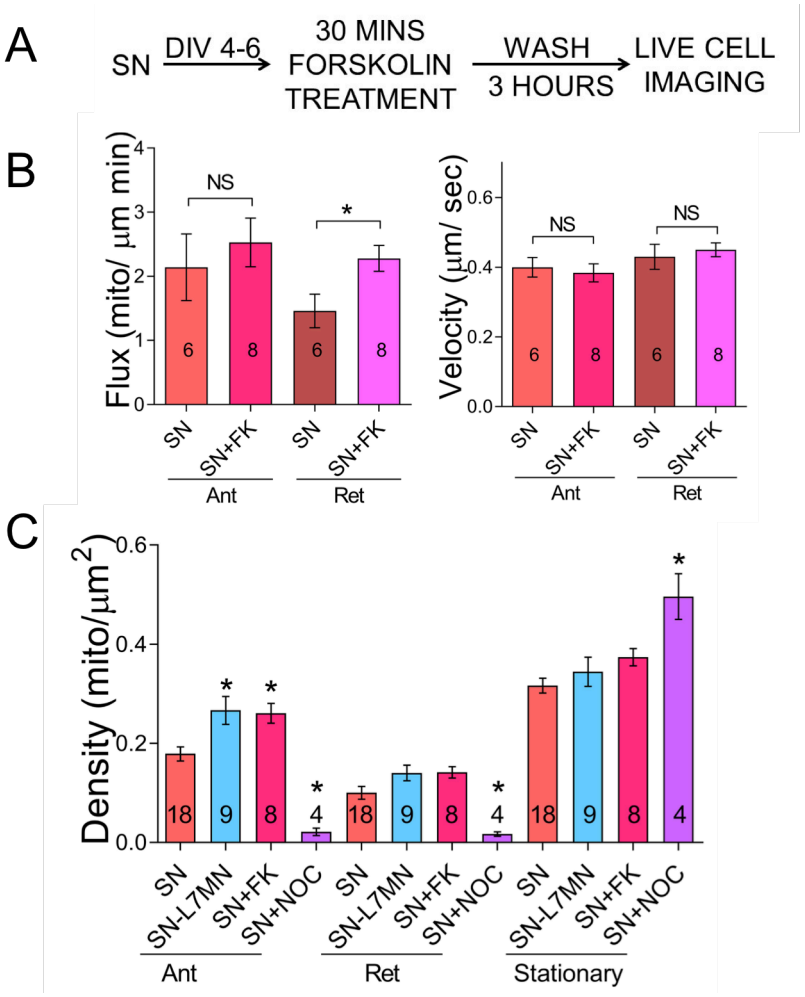

Supplementary Figure S2 Related to Figure 2. A: Experimental design schematics. **B:** Bar graphs showing measurements of flux and velocity of anterograde (Ant) and retrograde (Ret) transport after 3 hr after forskolin (FK) exposure. NS: non-significant. Numbers of neurons used are indicated in bar graphs. "*" is $p < 0.05$; Student's unpaired t test. **C.** Bar graph showing the density of mitochondria moving in the anterograde direction, retrograde direction or that are stationary. Values are shown in Supplementary Table S6. "*" is $p < 0.05$; One-way ANOVA and with post-hoc Tukey test. See also Table S1F.

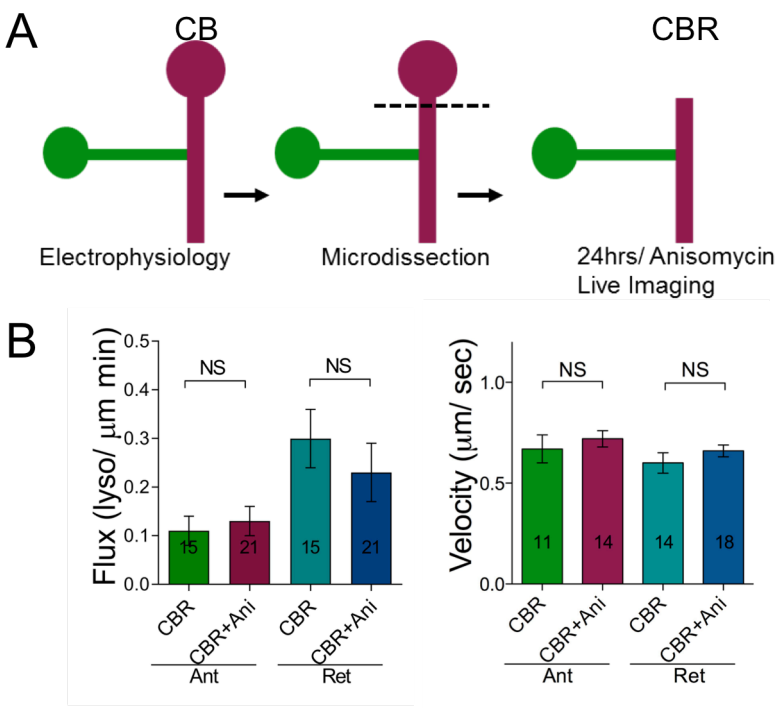

Supplementary Figure S3 Related to Figure 4. A. Experimental design schematics. **B.** Bar graphs showing measurements of flux and velocity of anterograde (Ant) and retrograde (Ret) transport of lysosomes in control and anisomycin (Ani) treated SN-L7MN where the cell body was removed (CBR) or with intact cell body (CB). Numbers of neurons used are indicated in bar graphs. NS: non-significant, Values are shown in Supplementary Table S7. "*" is $p < 0.05$; Student's unpaired t test. See also Table S1G.

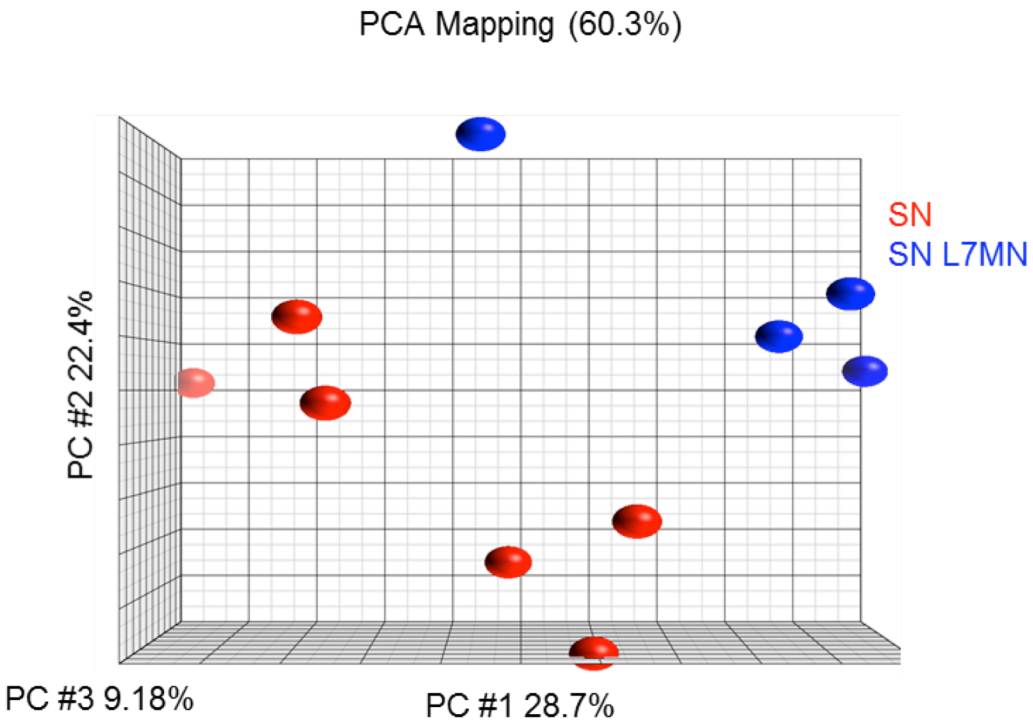

Supplementary Figure S4 Related to Figure 4. Principal Component Analysis (PCA) of microarray data showing the gene expression profiles in the SN cell body for neurons grown alone (n=4) or in the presence of L7MN (n=6). The figure shows the first two principal components of microarray analysis data (PC1, PC2, and PC3) in X, Y, and Z respectively.